

Agent-Centric Personalized Multiple Clustering with Multi-Modal LLMs

Ziye Chen^{1,2} Yiqun Duan^{1*} Riheng Zhu¹ Zhenbang Sun¹ Mingming Gong^{2*}
¹ TikTok, Australia

² School of Mathematics and Statistics, University of Melbourne, Australia

ziyecl@student.unimelb.edu.au, yiqunduan@bytedance.com, zhuriheng@bytedance.com,
 sunzhenbang@bytedance.com, mingming.gong@unimelb.edu.au

Abstract

Personalized multiple clustering aims to generate diverse partitions of a dataset based on different user-specific aspects, rather than a single clustering. It has recently drawn research interest for accommodating varying user preferences. Recent approaches primarily use CLIP embeddings with proxy learning to extract representations biased toward user clustering preferences. However, CLIP primarily focuses on coarse image-text alignment, lacking a deep contextual understanding of user interests. To overcome these limitations, we propose an agent-centric personalized clustering framework that leverages multi-modal large language models (MLLMs) as agents to comprehensively traverse a relational graph to search for clusters based on user interests. Due to the advanced reasoning mechanism of MLLMs, the obtained clusters align more closely with user-defined criteria than those obtained from CLIP-based representations. To reduce computational overhead, we shorten the agents' traversal path by constructing a relational graph using user-interest-biased embeddings extracted by MLLMs. A large number of weakly connected edges can be filtered out based on embedding similarity, facilitating an efficient traversal search for agents. Experimental results show that the proposed method achieves NMI scores of 0.9667 and 0.9481 on the Card Order and Card Suits benchmarks, respectively, largely improving the SOTA model by over 140%.

1. Introduction

Clustering is a fundamental technique in unsupervised learning that partitions data into meaningful groups, uncovering underlying structures within a dataset. Traditional clustering methods [3–5, 22] rely on handcrafted features or fixed representations, which may fail to capture

*Co-corresponding author. This work was completed by Ziye Chen during his internship at TikTok, Australia.

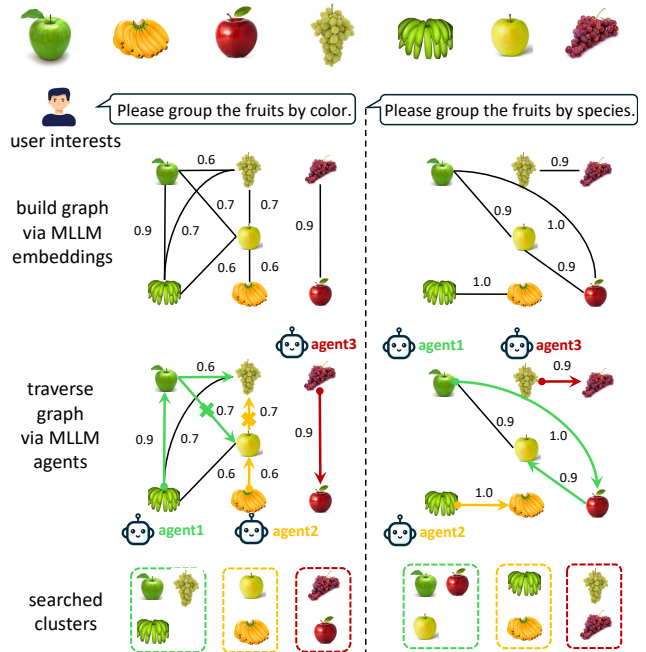


Figure 1. The workflow of the proposed agent-centric multiple clustering framework, which obtains a personalized clustering by using MLLMs as agents to traverse a relational graph based on user preferences. The relational graph is constructed from MLLM embeddings biased toward user interests.

the inherent complex data relationships. Recent advances [6, 14, 19, 23–25] leverage learning-based techniques to obtain more expressive representations, leading to significant performance improvements. Most of these approaches produce only one data partition from a single perspective.

However, real-world data exhibit inherent complexity, making it impossible for any single clustering method to capture all relevant structures. Consequently, identifying multiple valid clusterings within a dataset is essential to address various analytical needs. For example, the fruits in Fig. 1 can be grouped by color or species, depending on

the perspective. This need has driven the development of personalized multiple clustering, which aims to generate diverse partitions of a dataset based on different user preferences, rather than a single fixed solution.

Typical multiple clustering methods [21, 28, 35] primarily leverage autoencoders and data augmentation to extract diverse data representations, enabling clustering from different perspectives. However, identifying which clustering outcome aligns with user interests remains challenging, as these interests are often expressed through abstract keywords—such as color or species in the case of fruits, as illustrated in Fig. 1. Recent approaches [36, 37] integrate CLIP [15–17, 26] embeddings with proxy learning to obtain data representations tailored to user clustering preferences. While effective, CLIP is trained on coarse-grained image-text pair datasets and primarily focuses on direct modality alignment, lacking the deep contextual understanding necessary to capture abstract and complex user preferences. Furthermore, CLIP embeddings are derived from a fixed encoding of input images and predefined prompts, lacking the dynamic contextual reasoning needed to adapt to diverse and nuanced user interests.

To address these limitations, we propose an **agent-centric personalized multiple clustering framework** that leverages multi-modal large language models (MLLMs) as agents to directly assess data relationships and identify clusters based on user clustering preferences. Specifically, as shown in Fig. 1, we construct a relational graph with data points as nodes and their relationships as edges (discussed later), and then apply agents to comprehensively traverse the relational graph to search for clusters. By selecting high-degree nodes as starting points (which also serve as initial clusters), the agents iteratively expand the clusters through a decision-making process. At each step, they assess the membership of neighboring nodes in existing clusters according to user clustering preferences, and then adjust the cluster boundaries accordingly. Leveraging the advanced contextual understanding of MLLMs, our method produces clusters that more accurately reflect user-defined criteria compared to CLIP-based approaches.

A naive approach to construct the relational graph is to fully connect all nodes. However, this results in an overly dense graph, significantly increasing the traversal steps for agents and undermining the efficiency of cluster searching. To reduce computational overhead, we construct a weighted relational graph where edge weights are determined by the similarities between user-interest-biased embeddings extracted by MLLMs. By filtering out a large number of weakly connected edges based on embedding similarity, we shorten the agents’ traversal paths, allowing them to traverse the graph more efficiently. For each data point, the MLLM generates a user-interest-based description containing an embedding token, whose hidden states are projected

to form the data point’s embedding. Compared to CLIP-based embeddings, MLLM-based ones dynamically adapt to diverse and nuanced user interests through comprehensive contextual reasoning, preserving primarily valid edges and resulting in a sparser relational graph.

We evaluate our method on five publicly available visual datasets commonly used for multiple clustering tasks, and the results demonstrate its state-of-the-art performance. For instance, our method achieves NMI scores of 0.9667 and 0.9481 on the Card Order and Card Suits benchmarks, respectively, **surpassing the current state-of-the-art model by over 140%**. To the best of our knowledge, this is the first multiple clustering method built on MLLMs, providing a promising approach to unify personalized clustering and agent-based searching. The main contributions of our work can be summarized as follows:

- We introduce the first agent-centric personalized clustering framework that leverages multi-modal large language models (MLLMs) as agents to explore a relational graph extensively to identify clusters that accurately reflect user-specific interests.
- To enhance efficiency, we construct a relational graph using MLLM-generated embeddings that are tailored to user interests. By filtering out weakly connected edges based on embedding similarity, we significantly shorten the agents’ traversal paths during the search process.
- Experimental results demonstrate that our approach achieves substantial improvements on multiple benchmarks, demonstrating the effectiveness of our method.

2. Related Work

Multiple Clustering Multiple clustering explores diverse data partitions from different perspectives, gaining increasing attention. Early methods rely on hand-crafted rules and representations. For example, COALA [2] generates new clusters using existing ones as a constraint, Hu et al. [12] maximized eigengap across subspaces, and Dang et al. [7] utilizes an expectation-maximization framework to optimize mutual information. Recent approaches leverage learning-based techniques for better representations. For instance, ENRC [21] optimizes clustering objectives within a latent space learned by an auto-encoder, iMClusts [28] leverages auto-encoders and multi-head attention to learn diverse feature representations, and AugDMC [35] applies data augmentation to generate diverse image perspectives. However, it remains challenging to identify the clustering most relevant to user interests. Recently, Multi-MaP [37] and Multi-Sub [36] integrate CLIP embeddings with proxy learning to generate data representations aligned with user interests. While effective, CLIP lacks the deep contextual understanding necessary to capture abstract and nuanced user preferences.

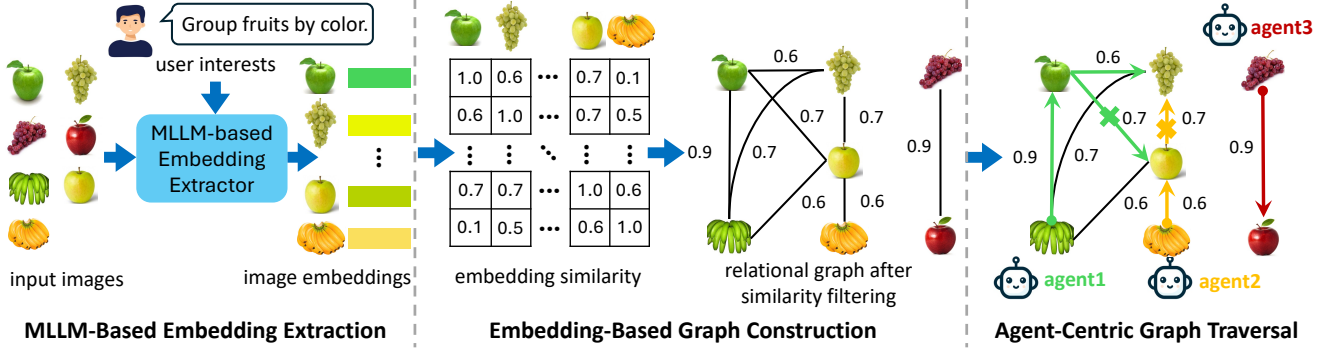


Figure 2. Overview of the agent-centric personalized multiple clustering framework. It begins by extracting image embeddings using an MLLM-based extractor guided by user interests. Next, a relational graph is constructed by computing pairwise similarities between image embeddings and filtering edges based on similarity thresholds. Finally, agent-centric graph traversal is performed, where multiple agents explore the relational graph to search for distinct clusters aligned with user clustering preferences.

LLM-Driven Agent Search LLM-driven agent search integrates Large Language Models (LLMs) into search processes, enabling agents to reason, plan, and interact with tools for efficient information retrieval. For example, PaSa [10] employs LLM-driven agents to search, read papers, and select references, ensuring comprehensive and accurate results for scholarly queries. Toolformer [29] demonstrates how LLMs can interact with external APIs (e.g., search engines, calculators) to enhance factual accuracy. ReAct [38] combines reasoning and acting, allowing agents to iteratively retrieve and process information for more effective decision-making. Recently, this field has shifted toward multi-agent search, emphasizing cooperative problem-solving, knowledge sharing, and decentralized decision-making. For example, CAMEL [13] introduces LLM agents with specialized roles (e.g., teacher and student) to refine search strategies collaboratively. Voyager [31] applies LLMs in an open-world exploration setting (Minecraft), where agents autonomously collect, analyze, and apply new knowledge. In this paper, we apply MLLM-driven agents to search clusters based on user interests.

3. Method

In this section, we introduce the proposed agent-centric personalized multiple clustering framework. We begin with an overview of the framework, followed by a detailed description of each component: agent-centric graph traversal, MLLM-based graph construction, and agent-based membership assessment.

3.1. Overall Framework

The framework, illustrated in Fig. 2, begins by extracting image embeddings using an MLLM-based embedding extractor, tailoring representations to user interests. A similarity matrix is then computed from these embeddings to construct a relational graph, where a large number of weakly

connected edges are filtered out based on embedding similarity. Finally, MLLM-based agents traverse this graph to search for clusters aligned with user clustering preferences, with each agent specializing in a different cluster. This agent-centric approach produces clusters that better adhere to user-defined criteria than those obtained from CLIP-based representations.

3.2. Agent-Centric Graph Traversal

In this section, we describe our agent-centric graph traversal approach for cluster discovery. We begin with a relational graph $\mathcal{G} = \{\mathcal{V}, \mathcal{E}, \mathcal{W}\}$ constructed as detailed in Sec 3.3, where each node $u \in \mathcal{V}$ represents a data point, and each edge $\{u, v\} \in \mathcal{E}$ carries a weight $w(u, v) \in \mathcal{W}$ indicating a precomputed, embedding-based similarity score between u and v . Leveraging multi-modal large language models (MLLMs) as agents, we traverse \mathcal{G} to search for clusters \mathcal{S} aligned with user interests T .

As outlined in Algorithm 1, we first identify the connected components of the relational graph \mathcal{G} , resulting in M components:

$$\{\mathcal{C}_i\}_{i=1}^M = \text{ConnectedComponents}(\mathcal{G}). \quad (1)$$

For each connected component \mathcal{C}_i , we select the highest-degree node v_i^* and designate it as the seed for an initial cluster \mathcal{S}_i as follows:

$$v_i^* = \arg \max_{v \in \mathcal{C}_i} \sum_{u \in \mathcal{N}(v)} w(v, u), \quad \mathcal{S}_i = \{v_i^*\}, \quad (2)$$

where $\mathcal{N}(v)$ is the neighborhood of node v . We then assign an MLLM-based agent \mathcal{A}_i to each initial cluster \mathcal{S}_i , resulting in a total of M agents, denoted as $\{\mathcal{A}_i\}_{i=1}^M$. Each agent \mathcal{A}_i iteratively expands its corresponding cluster \mathcal{S}_i by evaluating the membership of its neighboring nodes in \mathcal{S}_i based on user interests T .

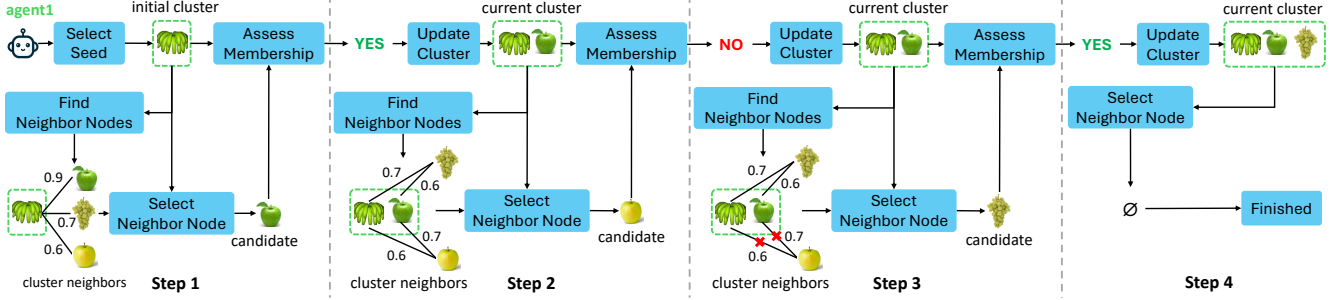


Figure 3. Illustration of the agent-centric graph traversal process for cluster searching. The agent begins with an initial cluster, selecting high-degree nodes as seeds, and expands it iteratively. At each step, it selects a neighboring node as a candidate based on embedding similarities, evaluates its membership in the current cluster according to the user’s clustering preferences, and updates the cluster accordingly. The process continues until no more suitable candidates are found.

As shown in Fig. 3 and Algorithm 1, at each step, the agent \mathcal{A}_i first determines the neighborhood of the current cluster \mathcal{S}_i , defined as:

$$\mathcal{N}(\mathcal{S}_i) = \bigcup_{v \in \mathcal{S}_i} \mathcal{N}(v) \setminus \mathcal{S}_i. \quad (3)$$

Next, the agent selects a candidate neighboring node v_j^* from $\mathcal{N}(\mathcal{S}_i)$ that exhibits the highest weighted connectivity to \mathcal{S}_i , given by:

$$v_j^* = \arg \max_{v \in \mathcal{N}(\mathcal{S}_i)} \sum_{u \in \mathcal{S}_i} w(v, u). \quad (4)$$

The agent then assesses whether v_j^* should be included in \mathcal{S}_i based on user-defined criteria, as detailed in Sec. 3.4. If the candidate node v_j^* is deemed a valid member, it is merged into the current cluster \mathcal{S}_i , updating \mathcal{S}_i as follows:

$$\mathcal{S}_i \leftarrow \mathcal{S}_i \cup \{v_j^*\}. \quad (5)$$

Otherwise, the edges between the candidate node v_j^* and the current cluster \mathcal{S}_i are removed from the edge set \mathcal{E} , yielding an updated edge set:

$$\mathcal{E} \leftarrow \mathcal{E} \setminus \{(u, v_j^*) \in \mathcal{E} \mid u \in \mathcal{S}_i\}. \quad (6)$$

The process from Eq. (3) to Eq. (6) is repeated until the neighborhood $\mathcal{N}(\mathcal{S}_i)$ is empty, at which point the final cluster \mathcal{S}_i is determined.

The M agents, $\{\mathcal{A}_i\}_{i=1}^M$, traverse the graph \mathcal{G} in parallel, each producing a cluster \mathcal{S}_i , resulting in a total of M clusters, $\{\mathcal{S}_i\}_{i=1}^M$. The cluster set \mathcal{S} (initially empty), node set \mathcal{V} , and edge set \mathcal{E} are then updated as follows:

$$\begin{aligned} \mathcal{S} &\leftarrow \mathcal{S} \cup \{\mathcal{S}_i\}_{i=1}^M, & \mathcal{V} &\leftarrow \mathcal{V} \setminus \bigcup_{i=1}^M \mathcal{S}_i, \\ \mathcal{E} &\leftarrow \mathcal{E} \setminus \{(u, v) \in \mathcal{E} \mid u, v \in \bigcup_{i=1}^M \mathcal{S}_i\} \end{aligned} \quad (7)$$

Algorithm 1: Agent-Centric Graph Traversal

Input: Relational graph $\mathcal{G} = (\mathcal{V}, \mathcal{E}, \mathcal{W})$, user interests T
Output: Final set of clusters \mathcal{S}
Initialize $\mathcal{S} \leftarrow \emptyset$
while $\mathcal{V} \neq \emptyset$ **do**
 $\{\mathcal{C}_1, \mathcal{C}_2, \dots, \mathcal{C}_M\} \leftarrow \text{ConnectedComponents}(\mathcal{G})$
 for $i \leftarrow 1$ **to** M **do**
 $v_i^* \leftarrow \arg \max_{v \in \mathcal{C}_i} \sum_{u \in \mathcal{N}(v)} w(v, u)$
 $\mathcal{S}_i \leftarrow \{v_i^*\}$ // Initialize cluster
 Assign agent \mathcal{A}_i to cluster \mathcal{S}_i
 $\mathcal{N}(\mathcal{S}_i) \leftarrow \bigcup_{v \in \mathcal{S}_i} \mathcal{N}(v) \setminus \mathcal{S}_i$
 while $\mathcal{N}(\mathcal{S}_i) \neq \emptyset$ **do**
 $v_j^* \leftarrow \arg \max_{v \in \mathcal{N}(\mathcal{S}_i)} \sum_{u \in \mathcal{S}_i} w(v, u)$
 if \mathcal{A}_i determines v_j^* belongs to \mathcal{S}_i based on T
 then
 $\mathcal{S}_i \leftarrow \mathcal{S}_i \cup \{v_j^*\}$
 else
 $\mathcal{E} \leftarrow \mathcal{E} \setminus \{(u, v_j^*) \in \mathcal{E} \mid u \in \mathcal{S}_i\}$
 $\mathcal{N}(\mathcal{S}_i) \leftarrow \bigcup_{v \in \mathcal{S}_i} \mathcal{N}(v) \setminus \mathcal{S}_i$
 $\mathcal{S} \leftarrow \mathcal{S} \cup \{\mathcal{S}_1, \mathcal{S}_2, \dots, \mathcal{S}_M\}$
 $\mathcal{V} \leftarrow \mathcal{V} \setminus \bigcup_{i=1}^M \mathcal{S}_i$
 $\mathcal{E} \leftarrow \mathcal{E} \setminus \{(u, v) \in \mathcal{E} \mid u, v \in \bigcup_{i=1}^M \mathcal{S}_i\}$
 $\mathcal{G} \leftarrow (\mathcal{V}, \mathcal{E}, \mathcal{W})$
return \mathcal{S}

The process from Eq. (1) to Eq. (7) is repeated iteratively until the node set \mathcal{V} becomes empty, at which point the final cluster set \mathcal{S} is obtained.

3.3. MLLM-Based Graph Construction

Here, we detail the construction of the relational graph $\mathcal{G} = (\mathcal{V}, \mathcal{E}, \mathcal{W})$ used for agent traversal. Each node $u \in \mathcal{V}$ corresponds to a data point. Each edge $(u, v) \in \mathcal{E}$ is assigned a weight $w(u, v) \in \mathcal{W}$, determined by the similarity between the embeddings $\mathcal{H}(u)$ and $\mathcal{H}(v)$. These embeddings are extracted by the MLLM for nodes u and v based on user interests T , as described below.

As shown in Fig. 4, we first design an embedding gen-

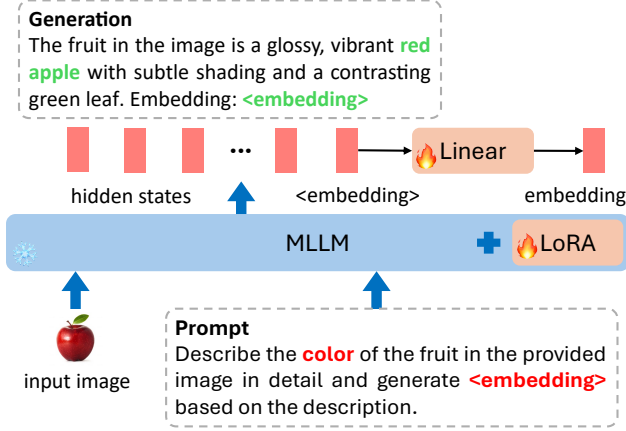


Figure 4. Illustration of image embedding extraction using MLLM based on user interests.

eration instruction based on user interests T . For example, if the user intends to cluster input images by “fruit color”, the instruction is formulated as: “Describe the color of the fruit in the provided image in detail and generate <embedding> based on the description.” We then provide the image u and the embedding instruction as input to the MLLM, which responds with a reasoning statement followed by an <embedding> token. For instance, it may generate: “The fruit in the image is a glossy, vibrant red apple with subtle shading and a contrasting green leaf. Embedding: <embedding>.” The hidden state of the <embedding> token in the output is then projected to obtain the user-interest-biased embedding $\mathcal{H}(u)$.

As shown in Fig. 2, after obtaining the embeddings $\mathcal{H}(u)$ and $\mathcal{H}(v)$, the edge weight $w(u, v)$ is computed as:

$$w(u, v) = \sigma(\beta \cdot \mathcal{H}(u)^\top \mathcal{H}(v)), \quad (8)$$

where β is a learnable logit scale, and σ denotes the sigmoid function. An edge (u, v) is retained in the edge set \mathcal{E} only if its weight $w(u, v)$ exceeds a predefined threshold τ . We fine-tune the MLLM using LoRA [11], with labels generated by GPT-4 [1]. For generation training, we use GPT-4’s descriptions of images under user interests T as labels, appending a <embedding> token. For embedding training, we supervise the similarity $w(u, v)$ based on GPT-4’s comparison of nodes u and v under user interests T .

3.4. Agent-Based Membership Assessment

Here, we describe how the agent \mathcal{A}_i assesses whether a candidate node v_j^* should be included in the current cluster \mathcal{S}_i based on user interests T . As shown in Fig. 5, we first select K representative nodes from \mathcal{S}_i , specifically those with the highest degree in \mathcal{S}_i , as follows:

$$\mathcal{R}_i = \arg \max_{\substack{R \subseteq \mathcal{S}_i \\ |\mathcal{R}| = \min(K, |\mathcal{S}_i|)}} \sum_{v \in R} \sum_{u \in \mathcal{N}(v) \cap \mathcal{S}_i} w(v, u), \quad (9)$$

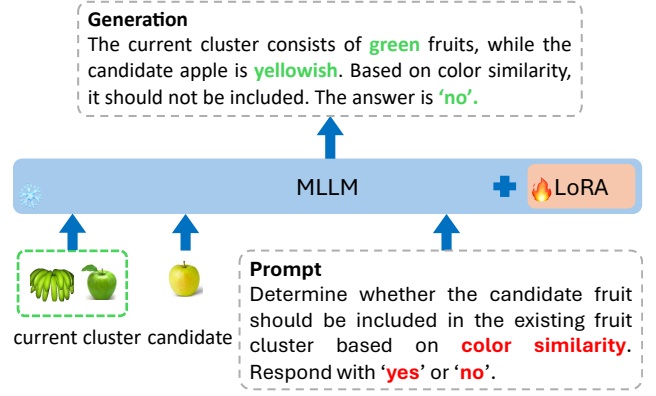


Figure 5. Illustration of how an agent evaluates a candidate node’s membership in the current cluster based on user interests.

where \mathcal{R}_i is the set of the selected representative nodes, which is used to represent the current cluster \mathcal{S}_i for agent-based membership assessment.

Then we design a membership assessment instruction based on user interests T . For example, if the user intends to cluster input images by “fruit color”, the instruction is formulated as: “Determine whether the candidate fruit should be included in the existing fruit cluster based on color similarity. Respond with ‘yes’ or ‘no’.” Next, we input the images along with the membership instruction into the agent \mathcal{A}_i , which generates a reasoning statement followed by a yes or no response. For example, it may generate: “The current cluster consists of green fruits, while the candidate apple is yellowish. Based on color similarity, it should not be included. The answer is ‘no’.” We refine the boundary of the current cluster \mathcal{S}_i based on the assessment of the agent \mathcal{A}_i , as outlined in Eqs. (5) and (6). For generation training, we fine-tune the MLLM-based agent \mathcal{A}_i using LoRA [11], where we use the corresponding membership assessment generated by GPT-4 [1] as labels.

4. Experiment

4.1. Datasets

We conduct experiments on five multiple-clustering benchmarks, including Card [35], CMUface [9], Fruit [12], Fruit360 [35], and CIFAR10-MC [36]. The Card dataset contains 8,029 images of playing cards, supporting two clustering schemes: order (from Ace to King) and suits (clubs, diamonds, hearts, spades). CMUface comprises 640 facial images with multiple clustering criteria, including face pose (left, right, straight, up), identity (20 people), presence of sunglasses (with, without), and emotion (angry, sad, happy, neutral). Fruit consists of 105 fruit images, which can be clustered by species (apples, bananas, grapes) or color (green, red, yellow). Fruit360 extends the Fruit

		Fruit		Fruit360		Card		CMUface				CIFAR10-MC	
		Color	Species	Color	Species	Order	Suits	Emotion	Sunglass	Identity	Pose	Type	Environment
MSC[12]	NMI	0.6886	0.1627	0.2544	0.2184	0.0807	0.0497	0.1284	0.1420	0.3892	0.3687	0.1547	0.1136
	RI	0.8051	0.6045	0.6054	0.5805	0.7805	0.3587	0.6736	0.5745	0.7326	0.6322	0.3296	0.3082
MCV[8]	NMI	0.6266	0.2733	0.3776	0.2985	0.0792	0.0430	0.1433	0.1201	0.4637	0.3254	0.1618	0.1379
	RI	0.7685	0.6597	0.6791	0.6176	0.7128	0.3638	0.5268	0.4905	0.6247	0.6028	0.3305	0.3344
ENRC[21]	NMI	0.7103	0.3187	0.4264	0.4142	0.1225	0.0676	0.1592	0.1493	0.5607	0.2290	0.1826	0.1892
	RI	0.8511	0.6536	0.6868	0.6984	0.7313	0.3801	0.6630	0.6209	0.7635	0.5029	0.3469	0.3599
iMClusts[28]	NMI	0.7351	0.3029	0.4097	0.3861	0.1144	0.0716	0.0422	0.1929	0.5109	0.4437	0.2040	0.1920
	RI	0.8632	0.6743	0.6841	0.6732	0.7658	0.3715	0.5932	0.5627	0.8260	0.6114	0.3695	0.3664
AugDMC[35]	NMI	0.8517	0.3546	0.4594	0.5139	0.1440	0.0873	0.0161	0.1039	0.5875	0.1320	0.2855	0.2927
	RI	0.9108	0.7399	0.7392	0.7430	0.8267	0.4228	0.5367	0.5361	0.8334	0.5517	0.4516	0.4689
DDMC[34]	NMI	0.8973	0.3764	0.4981	0.5292	0.1563	0.0933	0.1726	0.2261	0.6360	0.4526	0.3991	0.3782
	RI	0.9383	0.7621	0.7472	0.7703	0.8326	0.6469	0.7593	0.7663	0.8907	0.7904	0.5827	0.5547
Multi-Map[37]	NMI	0.8619	1.0000	0.6239	0.5284	0.3653	0.2734	0.1786	0.3402	0.6625	0.4693	0.4969	0.4598
	RI	0.9526	1.0000	0.8243	0.7582	0.8587	0.7039	0.7105	0.7068	0.9496	0.6624	0.7104	0.6737
Multi-Sub[36]	NMI	0.9693	1.0000	0.6654	0.6123	0.3921	0.3104	0.2053	0.4870	0.7441	0.5923	0.5271	0.4828
	RI	0.9964	1.0000	0.8821	0.8504	0.8842	0.7941	0.8527	0.8324	0.9834	0.8736	0.7394	0.7096
Ours	NMI	1.0000	1.0000	0.7214	0.6532	0.9667	0.9481	0.2196	0.9720	0.7631	0.7789	0.6385	0.5931
	RI	1.0000	1.0000	0.8715	0.8436	0.9952	0.9882	0.8415	0.9936	0.9763	0.9002	0.7812	0.7439

Table 1. Comparison with state-of-the-art methods across multiple clustering benchmarks. For methods that use k-means for clustering, the algorithm is run 10 times to account for its inherent randomness, with the average clustering performance reported. All methods are evaluated using two metrics: Normalized Mutual Information (NMI) and Rand Index (RI).

dataset with 4,856 images annotated for both species (apple, banana, grape, cherry) and color (green, red, yellow, burgundy). CIFAR10-MC includes 60,000 images with two clustering dimensions: type (transportation, animals) and environment (land, air, water).

4.2. Evaluation Metrics

We evaluate clustering performance using two widely adopted metrics: Normalized Mutual Information (NMI) [32] and Rand Index (RI) [27]. NMI quantifies mutual dependence between predicted and ground-truth clusters, normalized for cluster size variations. RI measures agreement between predicted and true partitions by considering correctly grouped and separated sample pairs. Both metrics range from 0 to 1, with higher values indicating better alignment with the ground truth.

4.3. Implementation Details

We adopt LLaVA [18] as our MLLM model, using Qwen2-7B [33] as the language model. To train the MLLM-based embedding extractor, we employ hard negative mining for data sampling, selecting 1,024 data pairs with the highest similarity entropy each epoch. GPT-4 then [1] evaluates the data pairs’ similarities based on user interests T , assigning labels accordingly. The embedding extractor is trained for 50 epochs. To train the MLLM-based agent, we uniformly sample a 1,024-node subgraph from the relational graph. GPT-4 then traverses this subgraph and assesses neighboring node memberships, providing labels accordingly. The

agent is trained for 50 epochs. We fine-tune only the language model with LoRA [11]. We use AdamW [20] for optimization with a learning rate of $1e^{-5}$, following a cosine decay schedule. In the relational graph construction, the embedding similarity threshold τ for filtering the weakly connected edges is set to 0.6.

4.4. Results

As shown in Table 1, our method outperforms state-of-the-art models across all multiple clustering benchmarks. On the Fruit dataset, it achieves perfect NMI and RI scores (1.0000) for both color-based and species-based clustering, outperforming all other methods. On the Fruit360 dataset, for color-based clustering, our method achieves an NMI of 0.7214, surpassing Multi-Map by 15.6% and Multi-Sub by 8.4%. For species-based clustering, it achieves an NMI of 0.6532, outperforming Multi-Map by 24.3% and Multi-Sub by 6.7%. On the CIFAR10-MC dataset, for type-based clustering, our method reaches an NMI of 0.6385 and an RI of 0.7812, surpassing Multi-Sub by 21.1% in NMI and 5.7% in RI. For environment-based clustering, it achieves an NMI of 0.5931 and an RI of 0.7439, surpassing Multi-Sub by 22.8% in NMI and 4.8% in RI.

On the Card dataset, for order-based clustering, our method achieves an NMI of 0.9667 and an RI of 0.9952, surpassing Multi-Sub by 146.5% in NMI and 12.6% in RI. For suits-based clustering, it achieves an NMI of 0.9481 and an RI of 0.9882, outperforming Multi-Sub by 205.4% in NMI and 24.4% in RI. On the CMUface dataset, for

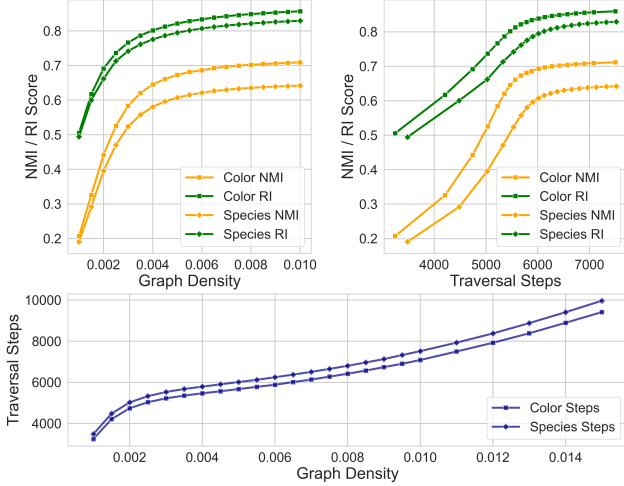


Figure 6. Graph density vs. clustering metrics and traversal steps.

sun-glass-based clustering, our method achieves an NMI of 0.9720 and an RI of 0.9936, surpassing Multi-Sub by 99.6% in NMI and 19.4% in RI. For pose-based clustering, it achieves an NMI of 0.7789 and an RI of 0.9002, surpassing Multi-Sub by 31.5% in NMI and 3.0% in RI. These significant improvements highlight the effectiveness of our agent-centric clustering framework in capturing user interests (e.g., order, suits, sunglasses, pose) with advanced contextual understanding from MLLMs, while minimizing interference from irrelevant information.

4.5. Ablation Studies

Density of Relational Graph. To assess the impact of graph density on agent graph traversal, we vary the embedding similarity threshold τ to generate relational graphs with different densities. The agents then traverse these graphs following Algorithm 1 to obtain comparative results. The experiments are conducted on the Fruit360 dataset. As shown in Fig. 6, increasing the graph density (i.e., relaxing the threshold τ) steadily improves the metrics of both color-based and species-based clustering (NMI and RI) until they begin to saturate. For example, the Color RI (green-square) and Species RI (green-diamond) curves quickly rise and plateau around 0.87 and 0.84, while the Color NMI (orange-square) and Species NMI (orange-diamond) converge near 0.72 and 0.65. This indicates that, once enough edges are retained to form connected subgraphs of semantically similar nodes, further densification of the graph yields only marginal gains in clustering accuracy.

However, the improved clustering performance comes at the expense of increased traversal cost. As the graph becomes denser, agents need to explore far more edges to accurately determine which nodes are true neighbors. In particular, the traversal-steps curve (darkblue) rises from

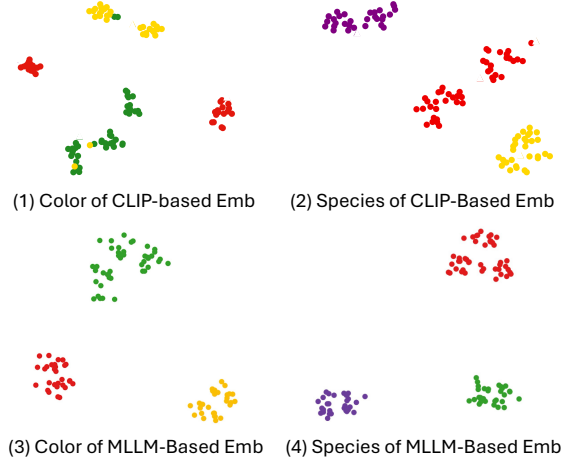


Figure 7. Visualization of MLLM-based and CLIP-based embeddings with corresponding labels on the Fruit dataset. For color-based embeddings, red, green, and yellow points correspond to fruits that are red, green, and yellow, respectively. For species-based embeddings, red, yellow, and purple points correspond to apples, bananas, and grapes, respectively.

roughly 3000 to nearly 10000 as the graph density is increased from 0.001 to 0.015, reflecting significantly greater computational overhead. Consequently, a moderate value of τ can strike a balance: the NMI/RI curves plateau beyond a certain graph density, so pushing the threshold τ to achieve this point improves efficiency without sacrificing meaningful gains in clustering performance. These results highlight the advantage of using *MLLM-based embeddings* for constructing the relational graph. By selectively pruning weakly connected edges with low embedding similarities, agents can avoid exhaustive searches in graph regions unlikely to contain relevant neighbors. Meanwhile, the context-aware nature of MLLM embeddings helps preserve essential edges between semantically similar nodes, ensuring high coherence with user interests while requiring fewer traversal steps than a fully dense graph.

MLLM-based vs. CLIP-based Embeddings. We validate the effectiveness of our MLLM-based embeddings by comparing them with CLIP-based ones across various clustering methods. We use Multi-Map [37] as the CLIP baseline, as both approaches decouple embedding extraction from clustering, enabling controlled ablations. As shown in Table 2, MLLM-based embeddings consistently outperform CLIP-based ones across all clustering methods. For instance, on the CMUface dataset (“Sun-glass” aspect), MLLM-based embeddings improve NMI from 0.3402, 0.3952 and 0.8456 to 0.7193, 0.7698 and 0.9720 for K-means, HDBSCAN and agent-centric clustering, respectively. These gains highlight the strong con-

Embedding	Dataset	Aspect	K-Means		HDBSCAN		Agent-Centric Graph Traversal		
			NMI	RI	NMI	RI	NMI	RI	Traversal Steps
CLIP Emb	Fruit360	Color	0.6239	0.8243	0.6541	0.8408	0.6922	0.8573	14821
		Species	0.5284	0.7582	0.5702	0.7851	0.6158	0.8180	14712
	Card	Order	0.3653	0.8587	0.4163	0.8708	0.8464	0.9679	29456
		Suits	0.2734	0.7039	0.3368	0.7275	0.8132	0.9313	14969
	CMUface	Sunglass	0.3402	0.7068	0.3952	0.7301	0.8456	0.9362	1281
		Pose	0.4693	0.6624	0.4935	0.6804	0.7168	0.8526	4015
MLLM Emb	Fruit360	Color	0.6629	0.8432	0.6912	0.8578	0.7214	0.8715	6404
		Species	0.5783	0.7924	0.6138	0.8179	0.6532	0.8436	6964
	Card	Order	0.7262	0.9406	0.7743	0.9515	0.9667	0.9952	12837
		Suits	0.6782	0.8745	0.7322	0.8972	0.9481	0.9882	9970
	CMUface	Sunglass	0.7193	0.9005	0.7698	0.9191	0.9720	0.9936	798
		Pose	0.6551	0.8051	0.6799	0.8241	0.7789	0.9002	1452

Table 2. Ablation study on the Fruit360, Card, and CMUface datasets. Agent-centric graph traversal clearly outperforms K-Means and HDBSCAN on both kinds of embeddings. Meanwhile, MLLM embeddings show significant advantages over CLIP embedding in reducing the traversal steps.

Dataset	Aspect	Metric	$K = 1$	$K = 2$	$K = 3$	$K = 4$
Fruit360	Color	NMI	0.7131	0.7185	0.7214	0.7240
		RI	0.8643	0.8691	0.8715	0.8730
	Species	NMI	0.6424	0.6490	0.6532	0.6559
		RI	0.8361	0.8402	0.8436	0.8457
Card	Order	NMI	0.9625	0.9652	0.9667	0.9673
		RI	0.9930	0.9943	0.9952	0.9957
	Suits	NMI	0.9421	0.9461	0.9481	0.9492
		RI	0.9860	0.9873	0.9882	0.9888

Table 3. Ablation study on number of representative nodes K .

textual reasoning capabilities of MLLMs, enabling them to better capture nuanced, user-specific preferences than CLIP. Fig. 7 further illustrates this via a t-SNE [30] visualization on the Fruit dataset: MLLM-based embeddings (bottom row) form compact, well-separated clusters, whereas CLIP-based embeddings (top row) show higher intra-cluster variance, especially in color-based partitioning. Thus, MLLM-based embeddings better capture user interests (e.g., color, species), improving clustering performance.

Furthermore, MLLM embeddings significantly reduce the number of traversal steps required for the convergence of agent-centric clustering. For instance, on the Fruit360 dataset (“Color” aspect), the agent traversal completes in 6404 steps by MLLM-based embeddings, roughly half of the 14821 steps needed by CLIP-based embeddings. This efficiency arises because MLLM-based embeddings produce a more sparse relational graph—many noise edges are correctly pruned due to lower similarities. Consequently, the agents can traverse fewer edges to expand clusters according to user clustering preferences, leading to both higher quality and more efficient clustering.

Agent-Centric Clustering vs. K-Means & HDBSCAN.

We evaluate the effectiveness of our agent-centric graph traversal clustering against classical K-Means and HDBSCAN. As shown in Table 2, the agent-centric approach consistently improves both NMI and RI across all datasets and embedding types. For instance, on the Card dataset (“Order” aspect) with MLLM-based embeddings, agent-centric clustering achieves an NMI of 0.9667, surpassing K-Means (0.7262) and HDBSCAN (0.7743). The gains are even more pronounced with CLIP-based embeddings. For example, on the Card dataset (“Order” aspect) with CLIP-based embeddings, agent-centric clustering achieves an NMI of 0.8464, outperforming K-Means (0.3653) and HDBSCAN (0.4163). Moreover, the agent-centric method often requires significantly fewer traversal steps with MLLM-based embeddings than with CLIP-based ones (as discussed above), enhancing efficiency.

Number of Representative Nodes. Table 3 shows the effect of varying K on clustering performance (NMI and RI). Using a single representative node may fail to capture the cluster’s diversity, leading to lower performance. Increasing K improves both metrics by better reflecting the cluster’s structure, although gains beyond three or four representatives are typically modest. Thus, a moderate K strikes the best balance between capturing diversity and avoiding redundant information.

5. Conclusion

This paper proposes an agent-centric clustering framework utilizing MLLMs to traverse relational graphs and identify clusters tailored to user interests. Leveraging MLLMs’ reasoning capabilities, our method better aligns clusters with user-defined criteria, surpassing CLIP embedding-based

techniques. For efficiency, we build relational graphs using user-interest-biased embeddings derived from MLLMs, guiding agents along optimized paths by filtering weak connections. Experiments show that our approach achieves state-of-the-art performance across multiple benchmarks, validating its effectiveness. The agent-centric clustering enables the customization of clustering criteria and can be extensively applied in industrial scenarios such as search and graph mining.

References

- [1] Josh Achiam, Steven Adler, Sandhini Agarwal, Lama Ahmad, Ilge Akkaya, Florencia Leoni Aleman, Diogo Almeida, Janko Altenschmidt, Sam Altman, Shyamal Anadkat, et al. Gpt-4 technical report. *arXiv preprint arXiv:2303.08774*, 2023. 5, 6
- [2] Eric Bae and James Bailey. Coala: A novel approach for the extraction of an alternate clustering of high quality and high dissimilarity. In *Sixth International Conference on Data Mining (ICDM'06)*, pages 53–62. IEEE, 2006. 2
- [3] Christopher M Bishop and Nasser M Nasrabadi. *Pattern recognition and machine learning*. Springer, 2006. 1
- [4] Mathilde Caron, Piotr Bojanowski, Armand Joulin, and Matthijs Douze. Deep clustering for unsupervised learning of visual features. In *Proceedings of the European conference on computer vision (ECCV)*, pages 132–149, 2018.
- [5] Mathilde Caron, Ishan Misra, Julien Mairal, Priya Goyal, Piotr Bojanowski, and Armand Joulin. Unsupervised learning of visual features by contrasting cluster assignments. *Advances in neural information processing systems*, 33:9912–9924, 2020. 1
- [6] Tianzhe Chu Chu, Shengbang Tong, Tianjiao Ding, Xili Dai, Benjamin Haeffele, Rene Vidal, and Yi Ma. Image clustering via the principle of rate reduction in the age of pretrained models. *International Conference on Learning Representations (ICLR)*, 2024. 1
- [7] Xuan Hong Dang and James Bailey. Generation of alternative clusterings using the cami approach. In *Proceedings of the 2010 SIAM International Conference on Data Mining*, pages 118–129. SIAM, 2010. 2
- [8] Joris Guérin and Byron Boots. Improving image clustering with multiple pretrained cnn feature extractors. *arXiv preprint arXiv:1807.07760*, 2018. 6
- [9] Stephan Günnemann, Ines Färber, Matthias Rüdiger, and Thomas Seidl. Smvc: semi-supervised multi-view clustering in subspace projections. In *Proceedings of the 20th ACM SIGKDD international conference on Knowledge discovery and data mining*, pages 253–262, 2014. 5
- [10] Yichen He, Guanhua Huang, Peiyuan Feng, Yuan Lin, Yuchen Zhang, Hang Li, et al. Pasa: An llm agent for comprehensive academic paper search. *arXiv preprint arXiv:2501.10120*, 2025. 3
- [11] Edward J Hu, Yelong Shen, Phillip Wallis, Zeyuan Allen-Zhu, Yuanzhi Li, Shean Wang, Lu Wang, Weizhu Chen, et al. Lora: Low-rank adaptation of large language models. *ICLR*, 1(2):3, 2022. 5, 6
- [12] Juhua Hu, Qi Qian, Jian Pei, Rong Jin, and Shenghuo Zhu. Finding multiple stable clusterings. *Knowledge and Information Systems*, 51:991–1021, 2017. 2, 5, 6
- [13] G Li, HAAK Hammoud, H Itani, D Khizbullin, and B Ghanem. Camel: communicative agents for” mind” exploration of large scale language model society.(2023). *arXiv preprint arXiv:2303.17760*. 3
- [14] Yunfan Li, Peng Hu, Zitao Liu, Dezhong Peng, Joey Tianyi Zhou, and Xi Peng. Contrastive clustering. In *Proceedings of the AAAI conference on artificial intelligence*, pages 8547–8555, 2021. 1
- [15] Yi Li, Hualiang Wang, Yiqun Duan, Hang Xu, and Xiaomeng Li. Exploring visual interpretability for contrastive language-image pre-training. *arXiv preprint arXiv:2209.07046*, 2022. 2
- [16] Yi Li, Hualiang Wang, Yiqun Duan, and Xiaomeng Li. Clip surgery for better explainability with enhancement in open-vocabulary tasks. *arXiv e-prints*, pages arXiv–2304, 2023.
- [17] Yi Li, Hualiang Wang, Yiqun Duan, Jiheng Zhang, and Xiaomeng Li. A closer look at the explainability of contrastive language-image pre-training. *Pattern Recognition*, page 111409, 2025. 2
- [18] Haotian Liu, Chunyuan Li, Qingyang Wu, and Yong Jae Lee. Visual instruction tuning. *Advances in neural information processing systems*, 36, 2024. 6
- [19] Yaroslava Lochman, Carl Olsson, and Christopher Zach. Learned trajectory embedding for subspace clustering. In *Proceedings of the IEEE/CVF Conference on Computer Vision and Pattern Recognition*, pages 19092–19102, 2024. 1
- [20] Ilya Loshchilov and Frank Hutter. Decoupled weight decay regularization. *arXiv preprint arXiv:1711.05101*, 2017. 6
- [21] Lukas Miklautz, Dominik Mautz, Muzaffer Can Altinigneli, Christian Böhm, and Claudia Plant. Deep embedded non-redundant clustering. In *Proceedings of the AAAI conference on artificial intelligence*, pages 5174–5181, 2020. 2, 6
- [22] Andrew Ng, Michael Jordan, and Yair Weiss. On spectral clustering: Analysis and an algorithm. *Advances in neural information processing systems*, 14, 2001. 1
- [23] Rabah Ouldnooghi, Chia-Wen Kuo, and Zsolt Kira. Clipgcd: Simple language guided generalized category discovery. *arXiv preprint arXiv:2305.10420*, 2023. 1
- [24] Qi Qian. Stable cluster discrimination for deep clustering. In *Proceedings of the IEEE/CVF International Conference on Computer Vision*, pages 16645–16654, 2023.
- [25] Qi Qian, Yuanhong Xu, Juhua Hu, Hao Li, and Rong Jin. Unsupervised visual representation learning by online constrained k-means. In *Proceedings of the IEEE/CVF Conference on Computer Vision and Pattern Recognition*, pages 16640–16649, 2022. 1
- [26] Alec Radford, Jong Wook Kim, Chris Hallacy, Aditya Ramesh, Gabriel Goh, Sandhini Agarwal, Girish Sastry, Amanda Askell, Pamela Mishkin, Jack Clark, et al. Learning transferable visual models from natural language supervision. In *International conference on machine learning*, pages 8748–8763. PMLR, 2021. 2
- [27] William M Rand. Objective criteria for the evaluation of clustering methods. *Journal of the American Statistical association*, 66(336):846–850, 1971. 6

- [28] Liangrui Ren, Guoxian Yu, Jun Wang, Lei Liu, Carlotta Domeniconi, and Xiangliang Zhang. A diversified attention model for interpretable multiple clusterings. *IEEE Transactions on Knowledge and Data Engineering*, 35(9):8852–8864, 2022. [2](#), [6](#)
- [29] Timo Schick, Jane Dwivedi-Yu, Roberto Dessi, Roberta Raileanu, Maria Lomeli, Eric Hambro, Luke Zettlemoyer, Nicola Cancedda, and Thomas Scialom. Toolformer: Language models can teach themselves to use tools. *Advances in Neural Information Processing Systems*, 36, 2024. [3](#)
- [30] Laurens Van der Maaten and Geoffrey Hinton. Visualizing data using t-sne. *Journal of machine learning research*, 9(11), 2008. [8](#)
- [31] Guanzhi Wang, Yuqi Xie, Yunfan Jiang, Ajay Mandlekar, Chaowei Xiao, Yuke Zhu, Linxi Fan, and Anima Anandkumar. Voyager: An open-ended embodied agent with large language models. *arXiv preprint arXiv:2305.16291*, 2023. [3](#)
- [32] JV White, Sam Steingold, and CG Fournelle. Performance metrics for group-detection algorithms. *Proceedings of Interface*, 2004:5, 2004. [6](#)
- [33] An Yang, Baosong Yang, Binyuan Hui, Bo Zheng, Bowen Yu, Chang Zhou, Chengpeng Li, Chengyuan Li, Dayiheng Liu, Fei Huang, Guanting Dong, Haoran Wei, Huan Lin, Jialong Tang, Jialin Wang, Jian Yang, Jiahong Tu, Jianwei Zhang, Jianxin Ma, Jianxin Yang, Jin Xu, Jingren Zhou, Jinze Bai, Jinzheng He, Junyang Lin, Kai Dang, Keming Lu, Keqin Chen, Kexin Yang, Mei Li, Mingfeng Xue, Na Ni, Pei Zhang, Peng Wang, Ru Peng, Rui Men, Ruize Gao, Runji Lin, Shijie Wang, Shuai Bai, Sinan Tan, Tianhang Zhu, Tianhao Li, Tianyu Liu, Wenbin Ge, Xiaodong Deng, Xiaohuan Zhou, Xingzhang Ren, Xinyu Zhang, Xipin Wei, Xuancheng Ren, Xuejing Liu, Yang Fan, Yang Yao, Yichang Zhang, Yu Wan, Yunfei Chu, Yuqiong Liu, Zeyu Cui, Zhenru Zhang, Zhifang Guo, and Zhihao Fan. Qwen2 technical report, 2024. [6](#)
- [34] Jiawei Yao and Juhua Hu. Dual-disentangled deep multiple clustering. In *Proceedings of the 2024 SIAM International Conference on Data Mining (SDM)*, pages 679–687. SIAM, 2024. [6](#)
- [35] Jiawei Yao, Enbei Liu, Maham Rashid, and Juhua Hu. Augdmc: Data augmentation guided deep multiple clustering. *Procedia Computer Science*, 222:571–580, 2023. [2](#), [5](#), [6](#)
- [36] Jiawei Yao, Qi Qian, and Juhua Hu. Customized multiple clustering via multi-modal subspace proxy learning. *arXiv preprint arXiv:2411.03978*, 2024. [2](#), [5](#), [6](#)
- [37] Jiawei Yao, Qi Qian, and Juhua Hu. Multi-modal proxy learning towards personalized visual multiple clustering. In *Proceedings of the IEEE/CVF Conference on Computer Vision and Pattern Recognition*, pages 14066–14075, 2024. [2](#), [6](#), [7](#)
- [38] Shunyu Yao, Jeffrey Zhao, Dian Yu, Nan Du, Izhak Shafran, Karthik Narasimhan, and Yuan Cao. React: Synergizing reasoning and acting in language models. *arXiv preprint arXiv:2210.03629*, 2022. [3](#)